

**Final Report:**  
**CFD Time-Integration Strategies for**  
**Large Chemical Systems**  
**F49620-03-1-0208**

William M. Eppard Ph.D.  
AeroSoft, Inc.  
1872 Pratt Drive, Suite 1275  
Blacksburg, VA 24060  
(540) 557-1910  
eppard@aerosft.com

March 29, 2006

**DISTRIBUTION STATEMENT A**  
Approved for Public Release  
Distribution Unlimited

**20060601068**

# REPORT DOCUMENTATION PAGE

Form Approved  
OMB No. 0704-0188

Public reporting burden for this collection of information is estimated to average 1 hour per response, including the time for reviewing instructions, searching existing data sources, gathering and maintaining the data needed, and completing and reviewing this collection of information. Send comments regarding this burden estimate or any other aspect of this collection of information, including suggestions for reducing this burden to Department of Defense, Washington Headquarters Services, Directorate for Information Operations and Reports (0704-0188), 1215 Jefferson Davis Highway, Suite 1204, Arlington, VA 22202-4302. Respondents should be aware that notwithstanding any other provision of law, no person shall be subject to a collection of information if it does not display a currently valid OMB control number. PLEASE DO NOT FORGET TO FILL IN YOUR FORM TO THE ABOVE ADDRESS.

1. REPORT DATE (DD-MM-YYYY) 29-March 2006		2. REPORT TYPE Final Performance Report		3. DATES COVERED (From - To) 1 Mar 2003 - 31 Dec 2004	
4. TITLE AND SUBTITLE  CFD Time-Integration Strategies for Large Chemical Systems				5a. CONTRACT NUMBER	
				5b. GRANT NUMBER F49620-03-1-0208	
				5c. PROGRAM ELEMENT NUMBER	
6. AUTHOR(S)  William M. Eppard				5d. PROJECT NUMBER	
				5e. TASK NUMBER	
				5f. WORK UNIT NUMBER	
7. PERFORMING ORGANIZATION NAME(S) AND ADDRESS(ES)  Aerosoft, Inc. 1872 Pratt Drive, Suite 1275 Blacksburg, VA 24060				8. PERFORMING ORGANIZATION REPORT NUMBER	
9. SPONSORING / MONITORING AGENCY NAME(S) AND ADDRESS(ES)  The Air Force Office of Scientific Research 875 N. Randolph Street, Suite 325, Room 3112 Arlington, VA 22203-1768 <i>Dr Farha Fahroo</i>				10. SPONSOR/MONITOR'S ACRONYM(S)  AFOSR/NM	
12. DISTRIBUTION / AVAILABILITY STATEMENT  Distribution A: Approved for Public Release; Distribution Unlimited				11. SPONSOR/MONITOR'S REPORT NUMBER(S)  AFRL-SR-AR-TR-06-0108	
13. SUPPLEMENTARY NOTES					
14. ABSTRACT To date, we have developed and implemented (into our GASP CFD Slow solver) a loosely-coupled strategy for the fluid-dynamic and chemical systems. The approach uses the lower-upper, symmetric, Gauss-Siedel (LU-SGS) implicit scheme to advance the fluid-dynamic system. In most cases, the chemical reactions have much smaller time scales than those associated with the flow, resulting in stiffness due to the source terms. Solution of the chemical system uses a time-operator splitting approach that allows isolation of the stiff source term from the transport terms. As a result, the solution process can be divided into two fractional steps - a transport fractional step and chemical production (or reaction) fractional step. The chemical transport fractional step is currently solved using a simple, low-cost Euler explicit scheme. The chemical production fractional step involves solving a system of ordinary differential equations representing the chemical source term and is carried out using a variable coefficient ordinary differential equation solver (DVODE).					
15. SUBJECT TERMS					
16. SECURITY CLASSIFICATION OF:				17. LIMITATION OF ABSTRACT	18. NUMBER OF
a. REPORT Unclassified	b. ABSTRACT Unclassified	c. THIS PAGE Unclassified	UL		19a. NAME OF RESPONSIBLE PERSON William Eppard
					19b. TELEPHONE NUMBER (include area code)

# 1 Objectives

Reacting flow simulations can be significantly improved through the utilization of detailed chemistry mechanisms. Two classes of problems that may benefit include chemical laser systems and hydrocarbon-fueled propulsion systems; each of which typically involve on the order of 50 to 200 chemical species, 200 rate equations, and time scales ranging from  $10^{-9}$  seconds to over 1 second. In general, implicit CFD algorithms are necessary to bypass chemical stiffness, but these schemes become very computationally demanding (both in terms of required memory and operation count) as the number of species grows. As a result, incorporation of detailed chemistry mechanisms into geometrically complex, turbulent CFD simulations becomes computationally prohibitive. Current approaches rely on reduced chemical mechanisms (*e.g.*, 20 to 30 species or less) which require considerable time and effort to develop and become less accurate with each simplification.

Our approach employs a loosely-coupled fluid-dynamic/chemistry formulation, that utilizes implicit solution methods for the fluid-dynamic equations and low-cost explicit or semi-implicit diagonal methods for the species continuity equations. The solution scheme for the chemical system (*i.e.*, the species continuity equations) utilizes a time-operator splitting method and a variable coefficient ordinary differential equation solver (DVODE) for the reaction fractional step to appropriately handle chemical stiffness. The DVODE solver appears to be very efficient, and this approach allows the use of less-expensive explicit or semi-implicit solution algorithms for the species transport fractional step. Our ultimate goal is to generalize, implement, and demonstrate (using our GASP CFD flow solver) that this scheme can be used to significantly reduce the costs associated with simulating complex flows with detailed chemical mechanisms.

# 2 Status of Effort

To date, we have developed and implemented (into our GASP CFD flow solver) a loosely-coupled strategy for the fluid-dynamic and chemical systems. The approach uses the lower-upper, symmetric, Gauss-Siedel (LU-SGS) implicit scheme to advance the fluid-dynamic system. In most cases, the chemical reactions have much smaller time scales than those associated with the flow, resulting in stiffness due to the source terms. Solution of the chemical system uses a time-operator splitting approach that allows isolation of the stiff source term from the transport terms. As a result, the solution process can be divided into two fractional steps - a transport fractional step and chemical production (or reaction) fractional step. The chemical transport fractional step is currently solved using the simple, low-cost Euler explicit scheme. The chemical production fractional step involves solving a system of ordinary differential equations representing the chemical source term and is carried out using a variable coefficient ordinary differential equation solver (DVODE). The DVODE solver has been integrated into the GASP CFD flow solver and appears to be very efficient. We have studied a number of steady-state flow problems, examining the usefulness of this scheme for reducing chemical stiffness and lowering computational costs. Our results indicate that the time-operator splitting approach with the DVODE solver represents a viable method for reducing chemical stiffness, allowing utilization of low-cost explicit and semi-implicit diagonal schemes for the chemical transport fractional step.

### 3 Accomplishments/New Findings

#### 3.1 GASP Governing Equations

GASP uses a cell-centered finite volume approach to solve the integral form of the Reynolds-Averaged Navier-Stokes equations:

$$\frac{\partial}{\partial t} \iiint_V \mathbf{Q} dV + \oint_S (\mathbf{F} - \mathbf{F}_v) \cdot \hat{\mathbf{n}} dS = \iiint_V \mathbf{W} dV. \quad (1)$$

The standard fluid-dynamic system has been augmented to include the effects of generalized chemistry, *i.e.*, the global continuity equation has been replaced with  $N$  species continuity equations to allow finite-rate chemical processes. The conserved-variable vector,  $\mathbf{Q}$ , the inviscid and viscous flux vectors,  $\mathbf{F}$  and  $\mathbf{F}_v$ , and the source-term vector,  $\mathbf{W}$ , are given as:

$$\mathbf{Q} = \begin{pmatrix} \rho_1 \\ \rho_2 \\ \vdots \\ \rho_N \\ \rho u_1 \\ \rho u_2 \\ \rho u_3 \\ \rho e_0 \end{pmatrix}, \quad \mathbf{F} = \begin{pmatrix} \rho_1 \mathbf{u} \\ \rho_2 \mathbf{u} \\ \vdots \\ \rho_N \mathbf{u} \\ \rho u_1 \mathbf{u} + p \hat{\mathbf{i}}_1 \\ \rho u_2 \mathbf{u} + p \hat{\mathbf{i}}_2 \\ \rho u_3 \mathbf{u} + p \hat{\mathbf{i}}_3 \\ \rho u h_0 \end{pmatrix}, \quad \mathbf{F}_v = \begin{pmatrix} -\rho_1 \mathbf{v}_d \\ -\rho_2 \mathbf{v}_d \\ \vdots \\ -\rho_N \mathbf{v}_d \\ \bar{\mathbf{T}} \cdot \hat{\mathbf{i}}_1 \\ \bar{\mathbf{T}} \cdot \hat{\mathbf{i}}_2 \\ \bar{\mathbf{T}} \cdot \hat{\mathbf{i}}_3 \\ -\mathbf{q} + \bar{\mathbf{T}} \cdot \mathbf{u} \end{pmatrix}, \quad \mathbf{W} = \begin{pmatrix} \omega_1 \\ \omega_2 \\ \vdots \\ \omega_N \\ 0 \\ 0 \\ 0 \\ 0 \end{pmatrix}.$$

Here,  $\bar{\mathbf{T}}$  is the stress tensor.

For a structured curvilinear coordinate system  $(\xi, \eta, \zeta)$ , the cell-centered, finite volume formulation for Eqn. (1) can be written as:

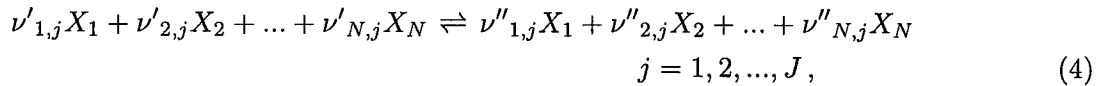
$$\frac{1}{J} \frac{\partial \mathbf{Q}}{\partial t} + \mathbf{R}(\mathbf{Q}) = 0 \quad (2)$$

where

$$\mathbf{R}(\mathbf{Q}) = \delta_\xi (\tilde{\mathbf{F}} - \tilde{\mathbf{F}}_v) + \delta_\eta (\tilde{\mathbf{G}} - \tilde{\mathbf{G}}_v) + \delta_\zeta (\tilde{\mathbf{H}} - \tilde{\mathbf{H}}_v) - \frac{1}{J} \mathbf{W}. \quad (3)$$

#### 3.2 Generalized Chemistry

GASP allows a general representation of chemical systems with  $N$  species and  $J$  reactions given by



where  $\nu'_{s,j}$  and  $\nu''_{s,j}$  are the stoichiometric coefficients of species  $X_s$  in the  $j$ th reaction. The rate of production of species  $s$ , denoted  $\omega_s$ , is given as

$$\omega_s \equiv \frac{d\rho_s}{dt} = \hat{M}_s \sum_{j=1}^J (\nu''_{s,j} - \nu'_{s,j}) \left[ k_{f,j} \prod_{l=1}^N \left( \frac{\rho_l}{\hat{M}_l} \right)^{\nu'_{l,j}} - k_{b,j} \prod_{l=1}^N \left( \frac{\rho_l}{\hat{M}_l} \right)^{\nu''_{l,j}} \right] \quad (5)$$

$s = 1, 2, \dots, N,$

where  $k_{f,j}$  and  $k_{b,j}$  are the forward and backward reaction rates. In GASP, the forward rates are determined from the Arrhenius equation

$$k_f = c T^\eta e^{-\epsilon/kT}, \quad (6)$$

and the backward rates are determined from the ratio of the forward to equilibrium rates

$$k_b = \frac{k_f}{k_c}. \quad (7)$$

The equilibrium rates are determined from either the Arrhenius equation, equilibrium curve fits, or from the McBride Curve fits and the minimization of Gibbs free energy.

### 3.3 Explicit Stability Bound

Explicit methods for solving flows with finite rate chemical kinetics are not practical because the time-step limit imposed by the explicit stability bound is too small to make the computation feasible. To examine this fact, we consider the linear scalar advection equation with a “chemical” source term:

$$\frac{\partial u}{\partial t} + a \frac{\partial u}{\partial x} = -\frac{u}{\tau_c}, \quad (8)$$

and the associated explicit, upwind ( $a > 0$ ) difference equation

$$\frac{\Delta_t u^n}{\Delta t} + a \frac{\nabla_x u_i}{\Delta x} = -\frac{u_i^n}{\tau_c}. \quad (9)$$

Here,  $\tau_c$  is the characteristic time for chemistry, and is representative of the time needed for the chemistry to reach equilibrium. Stability analysis produces two constraints: one based on the wave propagation (the CFL condition) and one based on the production of state. Specifically, we have

$$\begin{aligned} \Delta t &\leq \Delta x/a, \\ \Delta t &\leq 2\tau_c. \end{aligned}$$

The second constraint requires that the maximum stable time step decrease with decreasing chemical time scale ( $\tau_c$ ). This situation is labeled “chemical stiffness”, and corresponds to flow regions where the chemistry is near equilibrium, *i.e.*,  $\tau_c \rightarrow 0$ . The chemical time scale, for a given reaction, can be related to the reaction rate  $k$  through the following general relation

$$\tau_c = \frac{\omega}{k}, \quad (10)$$

where  $\omega$  is a function of species concentrations. Therefore, rapid chemical kinetics *i.e.*,  $k \rightarrow \infty$ , causes numerical stiffness because the numerical time step must approach zero in order to maintain stability.

#### 3.3.1 Implicit Schemes

In general, implicit algorithms bypass chemical stiffness by re-scaling the chemical time steps to accommodate the fastest reactions. The Euler implicit scheme as applied to Eqn. (2) is written as:

$$\left[ \frac{\mathbf{I}}{J\Delta t} + \delta_\xi(\tilde{\mathbf{A}} - \tilde{\mathbf{A}}_v) + \delta_\eta(\tilde{\mathbf{B}} - \tilde{\mathbf{B}}_v) + \delta_\zeta(\tilde{\mathbf{C}} - \tilde{\mathbf{C}}_v) - \frac{1}{J} \frac{\partial \mathbf{W}}{\partial \mathbf{Q}} \right] \Delta \mathbf{Q} = -\mathbf{R}(\mathbf{Q}), \quad (11)$$

Here,  $\tilde{\mathbf{A}}$ ,  $\tilde{\mathbf{B}}$ ,  $\tilde{\mathbf{C}}$ , represent the inviscid flux vector Jacobians,  $\tilde{\mathbf{A}}_v$ ,  $\tilde{\mathbf{B}}_v$ ,  $\tilde{\mathbf{C}}_v$ , are the viscous flux vector Jacobians, and  $\partial \mathbf{W}/\partial \mathbf{Q}$  is the source term Jacobian. Eqn. (11) represents a banded block  $(N + 4) \times (N + 4)$  matrix equation for  $\Delta \mathbf{Q}$ , where  $N$  is the number of chemical species. The band width is dependent on the choice of spatial discretization and the grid size. While implicit schemes

provide the fastest convergence rate, they are very computationally demanding, both in terms of memory requirements and operation count. For large numbers of species these schemes become computationally prohibitive. Fig. 1 shows the CPU time and memory required for the lower-upper, symmetric, Gauss-Siedel (LU-SGS) implicit scheme compared to the Euler explicit scheme on a  $20 \times 20 \times 20$  test grid using GASP. As an example, the CPU time/iteration for 60 species is 888 s for the LU-SGS algorithm while the corresponding CPU time/iteration for the Euler explicit scheme is 5.5 s, a factor of 161.4 times smaller. The required memory is 15.04 times smaller for the Euler explicit algorithm. Obviously, there is great incentive to utilize explicit or semi-implicit algorithms if the severe time-step limitation can be removed.

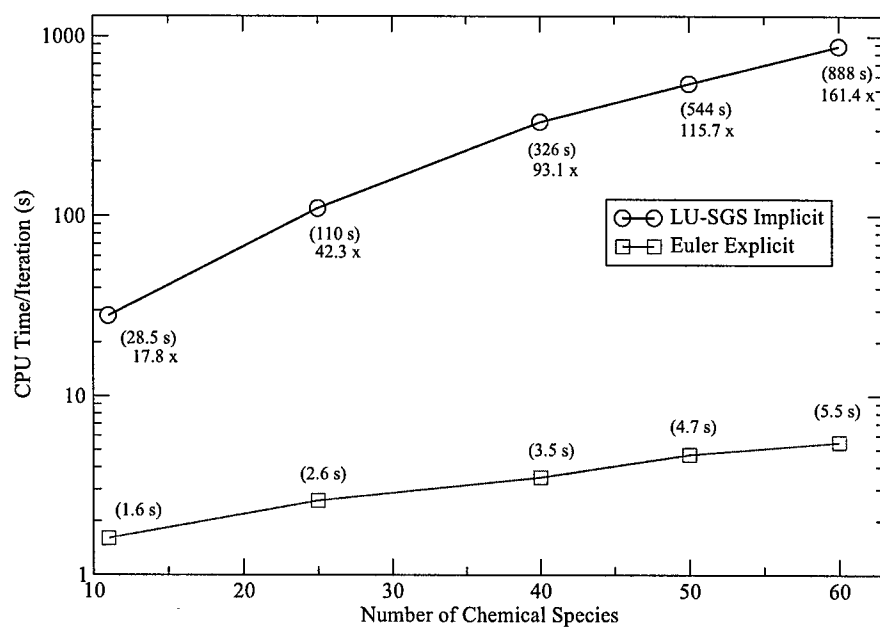
### 3.4 Loosely-Coupled Chemistry

The new time-integration strategy is based on a loosely-coupled fluid-dynamic/chemistry approach. This method allows solving the 5 fluid-dynamic equations (*i.e.*, the mixture continuity equation, 3 momentum equations, mixture energy equation, and two-equation turbulence if included) using implicit methods, with the possibility of solving the  $N$  species continuity equations using low-cost explicit or semi-implicit diagonal schemes. In the loosely-coupled approach, we partition the governing equations into two equation sets; a chemical set and a fluid-dynamic set. The partitioned conservative variable vector is given as follows:

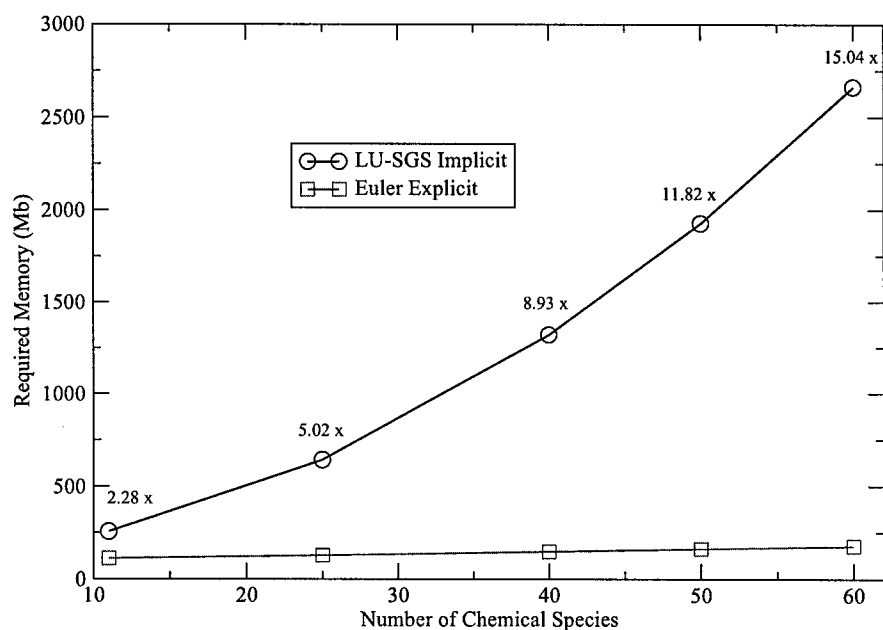
$$\mathbf{Q} = \left\{ \begin{array}{c} \mathbf{Q}_F \\ \dots \\ \mathbf{Q}_C \end{array} \right\} = \left\{ \begin{array}{c} \rho \\ \rho u_1 \\ \rho u_2 \\ \rho u_3 \\ \rho e_0 \\ \rho k \\ \rho \omega \\ \dots \\ \rho c_1 \\ \rho c_2 \\ \vdots \\ \rho c_N \end{array} \right\}.$$

Here  $c_i$  is the specie's mass fraction, (*i.e.*,  $c_i \equiv \rho_i/\rho$ ). In the first step of the loosely-coupled procedure, we update the fluid-dynamic system assuming constant mass fractions,  $c_i$ . At the end of this step the species densities,  $\rho_i'$ , are adjusted to reflect the changing mixture density as  $\rho_i' = \rho' c_i$ . In the second step, we solve the chemistry system (using the updated flow variables) for the individual specie's densities. During this step the mixture density is held constant, and the species mass fractions are determined as  $c_i = \rho c_i / \sum(\rho c_i)$ . This summation enforces the constraint that  $\sum c_i = 1$ . With this methodology, the fluid-dynamic system handles the global mass conservation while the chemistry system specifies the chemical composition. Using the loosely-coupled approach, the majority of the viscous terms are handled implicitly, with the exclusion of the species diffusion terms. This approach is expected to adequately reduce the viscous stability constraint for most problems. Our approach also allows for implicit boundary conditions for the fluid dynamic system.

In our recent work we have implemented the basic framework and tested the loosely-coupled scheme in GASP. Test cases show that the method convergences well and produces results consistent with the fully-coupled scheme.



(a) CPU Time per Iteration



(b) Required Memory

Figure 1: CPU time and memory requirements vs. the number of chemical species for the LU-SGS implicit and Euler explicit schemes on a  $20 \times 20 \times 20$  test grid.

### 3.5 Time-Operator Splitting

Solution of the chemical system uses a first-order, time-operator splitting approach that allows isolation of the stiff source term from the transport term. The chemistry system is written in terms of the transport and reaction components

$$\frac{1}{J} \frac{\partial \mathbf{Q}_C}{\partial t} + \mathbf{R}_{CT}(\mathbf{Q}) + \mathbf{R}_{CR}(\mathbf{Q}) = 0, \quad (12)$$

where  $\mathbf{R}_{CT}$  is the chemical transport residual and  $\mathbf{R}_{CR}$  represents the source term due to chemical reaction

$$\mathbf{R}_{CT}(\mathbf{Q}) = \delta_\xi(\tilde{\mathbf{F}}_C - \tilde{\mathbf{F}}_{C_v}) + \delta_\eta(\tilde{\mathbf{G}}_C - \tilde{\mathbf{G}}_{C_v}) + \delta_\zeta(\tilde{\mathbf{H}}_C - \tilde{\mathbf{H}}_{C_v}), \quad (13)$$

$$\mathbf{R}_{CR}(\mathbf{Q}) = -\frac{1}{J} \mathbf{W}. \quad (14)$$

The terms are then split, creating two systems of equations. Thus, a single step of the first order splitting method advancing the solution from time  $t^n$  to  $t^{n+1} = t^n + \Delta t$  amounts to an application of time discretizations applied to the system. The first step advances the transport system

$$\frac{1}{J} \frac{\partial \mathbf{Q}_C}{\partial t} + \mathbf{R}_{CT}(\mathbf{Q}) = 0, \quad (15)$$

from the initial condition  $\mathbf{Q}^n$  for a time  $\Delta t$ , and the solution is denoted  $\overline{\mathbf{Q}^{n+1}}$ . The second step advances the reaction system

$$\frac{1}{J} \frac{\partial \mathbf{Q}_C}{\partial t} + \mathbf{R}_{CR}(\mathbf{Q}) = 0, \quad (16)$$

from the initial condition  $\overline{\mathbf{Q}^{n+1}}$  for a time  $\Delta t$  to yield the final value  $\mathbf{Q}^{n+1}$ .

#### 3.5.1 Transport Fractional Step - Explicit Methods

The chemical transport fractional step (Eqn. (15)) is currently solved using the simple low-cost Euler explicit scheme. As applied to Eqn. (2) the Euler explicit scheme is written as

$$\mathbf{Q}^{n+1} = \mathbf{Q}^n - J \Delta t \mathbf{R}(\mathbf{Q}). \quad (17)$$

Future work utilizing semi-implicit diagonal schemes may be used to improve stability for the transport fractional step.

#### 3.5.2 Chemistry Fractional Step - DVODE

The chemical reaction fractional step (Eqn. (16)) has no spatial dependence and thus is essentially a system of ordinary differential equations at each node, requiring no boundary conditions. The chemical production fractional step is solved using the variable coefficient ordinary differential equation solver DVODE at each grid node. Input to the DVODE solver requires an estimate of whether or not the problem is stiff. If the problem is stiff DVODE utilizes Jacobians (either numerically generated or user-prescribed) otherwise if the problem is non-stiff DVODE utilizes efficient explicit procedures. In our implementation, we use an estimate of the local chemical Damkohler,  $Da$ , number to indicate chemical stiffness. At locations in the flow field where the Damkohler number is larger than some threshold value,  $Da^{\max}$ , we specify that the problem is stiff. This method allows DVODE to utilize Jacobians only where necessary, and should provide maximum efficiency for large numbers of species. Development of methods to compute the Damkoher number are discussed in the following sections.

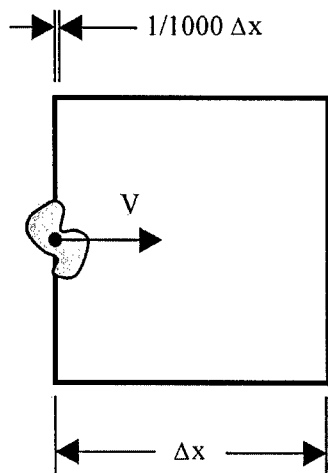


Figure 2: Fluid particle traveling across a cell.

### 3.5.3 Damkohler Number

The Damkohler number for chemistry is defined as the ratio of the fluid-dynamic to chemical time scales

$$Da \equiv \frac{\tau_{fd}}{\tau_c}. \quad (18)$$

A large Damkohler number ( $Da \gg 1$ ) means that the chemical time scale is much smaller than the fluid-dynamic scale, *i.e.*, the chemistry is tending toward equilibrium with the flow. Likewise, a small Damkohler number means the flow is nearly frozen, and chemical changes would be lagging far behind the fluid-dynamic changes. The local fluid-dynamic time scale,  $\tau_{fd}$ , is taken to be the time required for a fluid particle to advect across a cell. For the cell shown in Fig. 2 the fluid-dynamic time scale is  $\tau_{fd} = \Delta x/V$ , and we have

$$Da = \frac{\Delta x/V}{\omega/k}. \quad (19)$$

Large Damkohler numbers indicate fast chemical reactions and chemical stiffness.

#### Chemical Time Scales

Damkohler limiting is based on knowledge of the magnitude of the chemical times relative to the convective time of the flow (or physical time step for unsteady calculations). In this section we develop expressions that permit estimation of the characteristic chemical time scales for the elementary reactions that compose a chemical kinetics model (see Turns [3]). Notice that all chemical time scales can be written in the general form given by Eqn. (10).

The simplest possible reaction mechanism is the unimolecular reaction given by



This reaction occurs spontaneously by decomposition of a single molecule that has previously been activated to a high energy level by collision or otherwise. The corresponding rate equation for this reaction is

$$\frac{d[A]}{dt} = -k[A]. \quad (21)$$

Eqn. (21) can be integrated to yield the following result for the temporal decay of  $[A]$

$$\frac{[A]}{[A]_0} = \exp(-kt), \quad (22)$$

where  $[A]_0$  is the initial concentration of specie  $A$ . The *time constant*,  $\tau_c$ , is defined as the time elapsed for  $[A]$  to fall from its initial value to  $1/e$  times its initial value. Hence, we solve Eqn. (22) for the time when  $[A]/[A]_0 = 1/e$ , yielding the following chemical time constant

$$\tau_c = \frac{1}{k}. \quad (23)$$

As an example of a bimolecular reaction which occurs at a collision between two molecules, we consider the following reaction



and its rate equation

$$\frac{d[A]}{dt} = -k[A][B]. \quad (25)$$

We substitute the defect variable,  $x \equiv [A] - [A]_0 = [B] - [B]_0$ , into the rate equation and integrate to yield

$$\int \frac{dx}{(x + [A]_0)(x + [B]_0)} = -kt + C. \quad (26)$$

The left-hand integral can be determined to be

$$\int \frac{dx}{(x + [A]_0)(x + [B]_0)} = \frac{1}{[A]_0 - [B]_0} \ln \left( \frac{[B]}{[A]} \right). \quad (27)$$

and setting this result equal to the right-hand side of Eqn. (26), we can solve for the temporal decay of  $[A]/[B]$  as follows

$$\frac{[A]}{[B]} = \frac{[A]_0}{[B]_0} \exp \{ ([A]_0 - [B]_0) kt \}. \quad (28)$$

This expression is used to determine the time constant for the decay of the specie concentrations. Assigning  $[A]_0$  to be the smaller of the two concentrations, we solve Eqn. (28) for  $\tau_c$  by solving for the time when  $[A]/[A]_0 = 1/e$  where we use the fact that  $[B]/[B]_0 = ([A]_0/[B]_0)([A]/[A]_0 - 1) + 1$ . We obtain the time constant for the bimolecular reaction as

$$\tau_c = \frac{\mathcal{L}\{[A]_0/[B]_0\}}{([A]_0 - [B]_0)k} \quad (29)$$

where

$$\mathcal{L}(x) = -\ln[e - (e - 1)x] \quad (30)$$

and

$$\mathcal{L}\{[A]_0/[B]_0\} \equiv \ln \left. \frac{[A]/[A]_0}{[B]/[B]_0} \right|_{[A]/[A]_0=1/e} = -\ln \left[ e - (e - 1) \left( \frac{[A]_0}{[B]_0} \right) \right]. \quad (31)$$

As an example of a termolecular reaction which occurs at a collision between three molecules, we consider the following reaction



and its rate equation

$$\frac{d[A]}{dt} = -k [A]^2 [B]. \quad (33)$$

We again substitute the defect variable,  $x \equiv [A] - [A]_0 = [B] - [B]_0$ , into the rate equation and integrate to yield

$$\int \frac{dx}{(x + [A]_0)^2 (x + [B]_0)} = -kt + C. \quad (34)$$

In this case the temporal decay of  $[A]/[B]$  becomes

$$\frac{[A]}{[B]} = \frac{[A]_0}{[B]_0} \exp \left\{ ([A]_0 - [B]_0)^2 kt + \left( 1 - \frac{[B]_0}{[A]_0} \right) \left( \frac{[A]_0}{[A]} - 1 \right) \right\}. \quad (35)$$

This expression is used to determine the time constant for the decay of the specie concentrations. For the case where  $[A]_0$  is the smaller of the two concentrations, we solve Eqn. (35) for  $\tau_c$  by solving for the time when  $[A]/[A]_0 = 1/e$  where we use the fact that  $[B]/[B]_0 = ([A]_0/[B]_0)([A]/[A]_0 - 1) + 1$ . We obtain the time constant for the termolecular reaction as

$$\tau_c = \frac{\mathcal{L}\{[A]_0/[B]_0\} - \mathcal{F}\{[A]_0/[B]_0\}}{([A]_0 - [B]_0)^2 k} \quad (36)$$

where

$$\mathcal{F}(x) = \left( 1 - \frac{1}{x} \right) (e - 1) \quad (37)$$

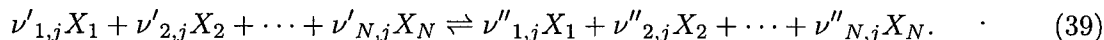
and

$$\mathcal{L}\{[A]_0/[B]_0\} \equiv \left( 1 - \frac{[B]_0}{[A]_0} \right) \left( \frac{[A]_0}{[A]} - 1 \right) \Big|_{[A]/[A]_0=1/e} = \left( 1 - \frac{[B]_0}{[A]_0} \right) (e - 1). \quad (38)$$

Table 1 lists the chemical time scales for several common elementary reactions.

### A General Method for Computing the Chemical Time Constant

As demonstrated above, the analytical expression for the chemical time constant depends on the form of the elementary reaction. Rather than devise expressions for every possible reaction, we have developed a general method which applies to every case. In the context of Eqn. (4), consider the  $j^{th}$  chemical reaction in a general chemical-kinetics model



The defect law for each specie can be written as follows

$$\frac{[X_1] - [X_1]_0}{\nu''_{1,j} - \nu'_{1,j}} = \frac{[X_2] - [X_2]_0}{\nu''_{2,j} - \nu'_{2,j}} = \cdots = \frac{[X_N] - [X_N]_0}{\nu''_{N,j} - \nu'_{N,j}}. \quad (40)$$

We can compute the chemical time scale numerically by solving an ordinary differential equation for the specie with the smallest negative defect. That is, we assume that  $\nu_{1,j} \equiv \nu''_{1,j} - \nu'_{1,j} < 0$  and that the species are listed in order of increasing defect

$$\frac{[X_1]_0}{|\nu_{1,j}|} < \frac{[X_2]_0}{|\nu_{2,j}|} < \cdots < \frac{[X_N]_0}{|\nu_{N,j}|}. \quad (41)$$

Under these conditions, we can solve the following ODE for the decay of  $[X_1]$

$$\frac{d[X_1]}{dt} = \nu_{1,j} k_{f,j} [X_1]^{\nu'_{1,j}} [X_2]^{\nu'_{2,j}} \cdots [X_N]^{\nu'_{N,j}}. \quad (42)$$

Reaction	Example	$\tau_c$
$A \rightarrow \text{products}$	$I_2^* \rightarrow 2 I$	$\frac{1}{k}$
$A + M \rightarrow \text{products} + M$	$H_2O + M \rightarrow H + OH + M$	$\frac{1}{[M] k}$
$2 A \rightarrow \text{products}$	$2 O \rightarrow O_2$	$\frac{e - 1}{2[A]_0 k}$
$2 A \rightarrow \text{products} + A$	$2 O_2 \rightarrow 2 O + O_2$	$\frac{e - 1}{[A]_0 k}$
$2 A + M \rightarrow \text{products} + M$	$2 H + M \rightarrow H_2 + M$	$\frac{e - 1}{2[A]_0[M] k}$
$3 A \rightarrow \text{products}$	$3 I \rightarrow I_2 + I^*$	$\frac{e^2 - 1}{6[A]_0^2 k}$
$3 A \rightarrow \text{products} + A$	$3 H \rightarrow H_2 + H$	$\frac{e^2 - 1}{4[A]_0^2 k}$
$A + B \rightarrow \text{products}$	$H_2 + O_2 \rightarrow 2 HO$	$\frac{\mathcal{L}(x)}{([A]_0 - [B]_0) k}$
$A + B + M \rightarrow \text{products} + M$	$N + O + M \rightarrow NO + M$	$\frac{\mathcal{L}(x)}{([A]_0 - [B]_0)[M] k}$
$2 A + B \rightarrow \text{products} + A$	$2 H + OH \rightarrow H_2O + H$	$\frac{\mathcal{L}(x) - \mathcal{F}(x)}{([A]_0 - [B]_0)^2 k}$
$2 A + B \rightarrow \text{products}$	$2 H_2 + O_2 \rightarrow 2 H_2O$	$\frac{\mathcal{L}(x') - \mathcal{F}(x')}{([A]_0 - [B]_0)^2 k}$

Table 1: Chemical time constants where  $x \equiv [A]_0/[B]_0$  and  $A$  is assigned to the specie with the smaller initial concentration where interchangeable. The second to last reaction assumes that  $[A]_0 < [B]_0$ , and the last reaction uses  $x' \equiv [A]_0/2[B]_0$  and assumes  $[A]_0 < 2[B]_0$ .

The defect law (Eqn. (40)) can be used to write all the specie concentrations if Eqn. (42) in terms of  $[X_1]$ . A similar ODE can be written for the smallest decreasing specie in the backward reaction with rate coefficient  $k_{b,j}$ .

To solve Eqn. (42) for the chemical time scale we use a second order mid-point method to determine the time when the specie decays by a ratio of  $1/e$ . We first make a first-order approximation using the Euler-explicit method for an initial guess

$$[X_1]^* = [X_1]_0 + \left[ \frac{d[X_1]}{dt} \right]_0 \tau_{ch}^* \quad (43)$$

Solving for  $\tau_{ch}^*$  and noting that  $[X_1]^*/[X_1]_0 = 1/e$ , we have

$$\tau_{ch}^* = \left( [X_1]_0 / \left[ \frac{d[X_1]}{dt} \right]_0 \right) (1/e - 1). \quad (44)$$

The second-order approximation can be written by re-evaluating the right hand side of Eqn. (42) using the mid-point concentration (*i.e.*,  $[X_1]_0 + [X_1]'_0 (1/2 \tau_{ch}^*)$ ). Our chemical time scale for any elementary reaction can then be written as

$$\tau_{ch} = \left( [X_1]_0 / \left[ \frac{d[X_1]}{dt} \right]_{1/2 \tau_{ch}^*} \right) (1/e - 1). \quad (45)$$

### Fluid-Dynamic Time Scales

The fluid-dynamic time scale is determined locally for each cell in the flow field. For a structured curvilinear coordinate system  $(\xi, \eta, \zeta)$ , we compute a characteristic fluid-dynamic time for each coordinate direction

$$\tau_{fd \xi}^{-1} = \frac{1}{2} \left( |\tilde{u}_{i-1/2}| \frac{A_{i-1/2}}{V_{i,j,k}} + |\tilde{u}_{i+1/2}| \frac{A_{i+1/2}}{V_{i,j,k}} \right) \quad (46)$$

$$\tau_{fd \eta}^{-1} = \frac{1}{2} \left( |\tilde{u}_{j-1/2}| \frac{A_{j-1/2}}{V_{i,j,k}} + |\tilde{u}_{j+1/2}| \frac{A_{j+1/2}}{V_{i,j,k}} \right) \quad (47)$$

$$\tau_{fd \zeta}^{-1} = \frac{1}{2} \left( |\tilde{u}_{k-1/2}| \frac{A_{k-1/2}}{V_{i,j,k}} + |\tilde{u}_{k+1/2}| \frac{A_{k+1/2}}{V_{i,j,k}} \right). \quad (48)$$

Here  $\tilde{u}$  is the contravariant velocity on each face given as

$$\tilde{u} = \mathbf{u} \cdot \bar{\nabla} \tilde{k} \quad (k = \xi, \eta, \zeta), \quad (49)$$

where  $\bar{\nabla} \tilde{k}$  is the face unit normal. The fluid-dynamic time scale is taken as the minimum of each of the directional times

$$\tau_{fd} = \min\{\tau_{fd\xi}, \tau_{fd\eta}, \tau_{fd\zeta}\}. \quad (50)$$

## 3.6 Results

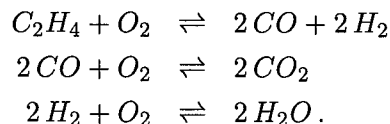
### 3.6.1 Ethylene Flow over Blunt Body

As a test case, we model the supersonic flow of ethylene ( $C_2H_4$ ) around a blunt body using the 7-specie, chemical-kinetics model of Baurle *et al.* [1]. A  $31 \times 26$  mesh is generated around an axis-symmetric body traveling at  $M_\infty = 7.46$ . The free-stream pressure is  $p_\infty = 42,657 \text{ N/m}^2$  and the

densities which correspond to an equivalence ratio of  $\phi = 1.667$  are

$$\begin{aligned}\rho_{C_2H_4} &= 0.0404635 \text{ kg/m}^3 \\ \rho_{O_2} &= 0.0830436 \text{ kg/m}^3 \\ \rho_{N_2} &= 0.2734928 \text{ kg/m}^3.\end{aligned}$$

The Baurle reaction mechanism is given as



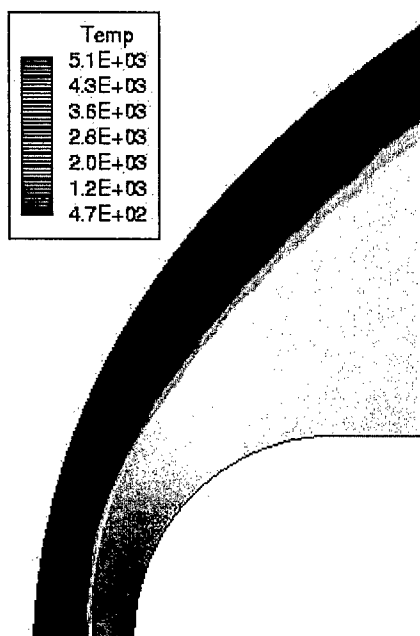
The resulting flow solution is shown in terms of temperature contours (Fig. 3(a)) and  $H_2O$  mass fraction contours (Fig. 3(b)). As the flow passes through the bow shock, the increased temperature ignites the ethylene mixture and results in a reaction front indicated by the  $H_2O$  mass-fraction contours. Fig. 3(c) shows contours of the Damkohler number for this problem. The Damkohler number is largest near the stagnation point, reaching a maximum value of  $Da = 2223.84$ . A significant portion of the flow field has Damkohler numbers exceeding  $Da = 100$ . We ran two calculations; a fully coupled case, and a loosely coupled case with operator splitting and the DVODE solver for the chemistry system. Jacobians were utilized in the DVODE solver for Damkohler numbers greater than  $Da^{\max} = 25$ . Utilizing the loosely-coupled scheme with operator splitting, we have been able to obtain solutions to the ethylene blunt nose problem using the low-cost Euler explicit scheme for chemistry transport. Fig. 4 shows good agreement for the water mass fraction along the stagnation line for both schemes. Without the operator splitting approach, the Euler explicit scheme applied to the complete chemistry system diverged for all tested time steps.

### 3.6.2 Hydrogen-Air Wedge

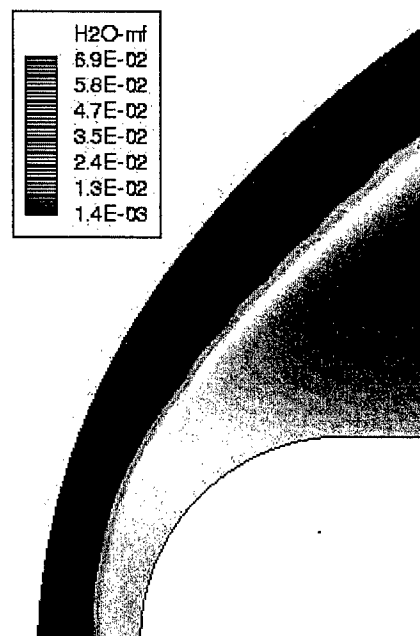
In a second test case we consider the two-dimensional, inviscid simulation of Mach  $M = 5.189$ , premixed hydrogen air flow over a 20 deg wedge. The grid size is  $101 \times 61$  and we utilize the 7-species  $H_2$ -Air model of Drummond [2]. In the present study, the inflow mixture is fuel-lean, with an equivalence ratio of  $\phi = 0.75$ . The free-stream conditions are

$$\begin{aligned}\rho_{N_2} &= 0.2374175 \text{ kg/m}^3 \\ \rho_{O_2} &= 0.0720856 \text{ kg/m}^3 \\ \rho_{H_2} &= 0.0068121 \text{ kg/m}^3 \\ T &= 800 \text{ K} \\ V &= 3300 \text{ m/s} \\ p &= 93.825 \text{ kN/m}^2 \\ M &= 5.189.\end{aligned}$$

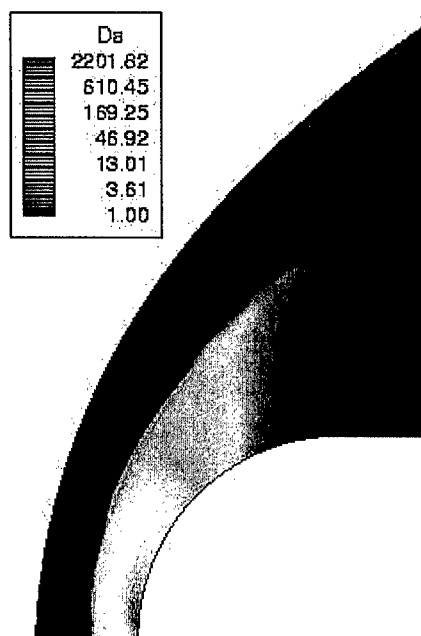
Again, we ran two calculations: a fully coupled case, and a loosely coupled case with operator splitting and the ODE solver for the chemistry system. The calculation was run with Van Leer flux vector splitting and third-order spatial accuracy. Fig. 5 shows contours of temperature,  $H_2O$  fractions, and Damkohler number for this problem. As the flow passes through the shock, the increased temperature ignites the  $H_2$ -Air mixture. The flame front occurs downstream of the oblique shock, and is indicated by the increase in water mass fraction. Ignition occurs a significant distance (*i.e.*, the induction



(a) Temperature.



(b)  $H_2O$  Mass fraction.



(c) Damkohler number.

Figure 3: Contours of temperature,  $H_2O$  mass fraction, and  $Da$  number for the ethylene blunt-body flow.

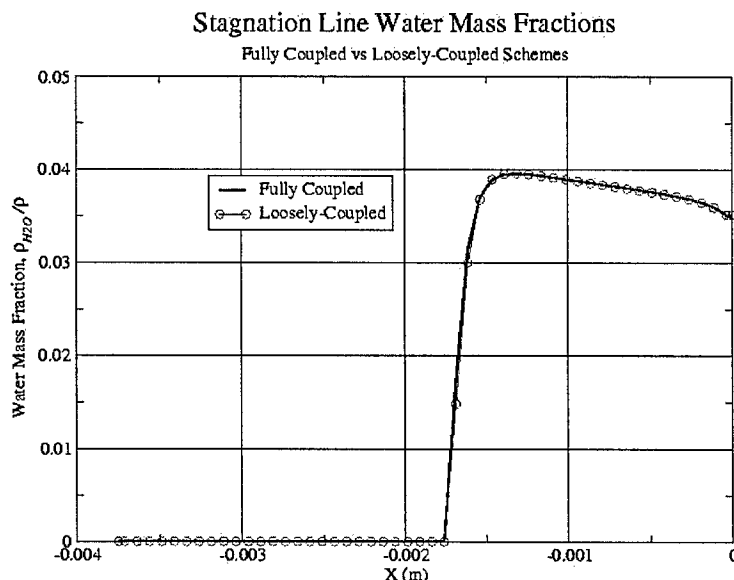


Figure 4:  $H_2O$  mass fractions along the stagnation line for the ethylene blunt-body flow.

distance) downstream of the shock due to the finite characteristic time for chemical reaction and high flow velocity. This causes a separation between the shock and flame front called the induction zone.

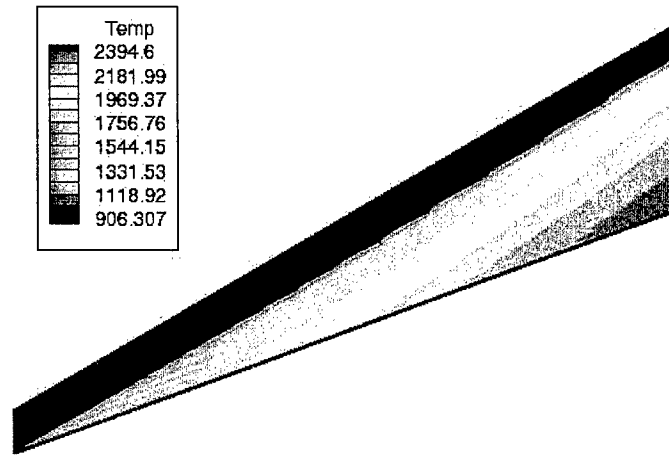
Both solutions are essentially converged after 2000 iterations. Fig. 6 shows the temperature and  $H_2O$  mass-fraction profiles along the  $j = 41$  grid line for both schemes. The results show very good agreement between the loosely-coupled fully-coupled solutions. Convergence hangs up slightly for the loosely-coupled scheme, but both solutions converge nearly three orders which is typical of higher-order solutions (see Fig. 7). For the 7-species case the fully-coupled approach required 7,508 s while the loosely-coupled approach required 4,940 s, a speed up factor of 1.52. To examine potential savings for larger chemical systems, we scaled the chemistry model to include up to 20 species by adding inert species. For the 20-species case the fully-coupled approach required 40,485 s while the loosely-coupled approach required 11,706 s, a speed up factor of 3.46.

### 3.6.3 2-D COIL Simulation

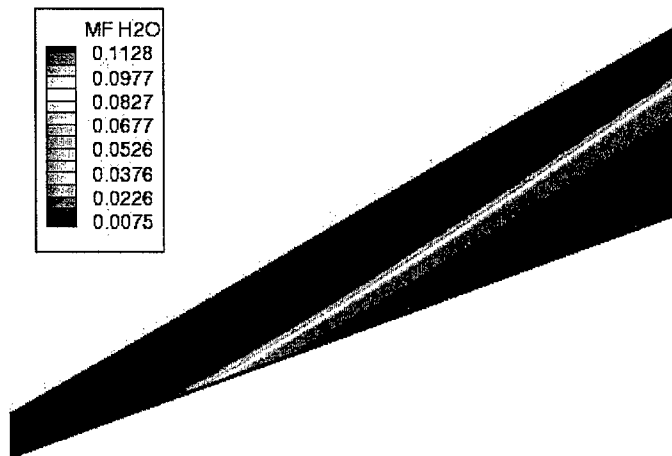
As a final test case we have run a 2-D COIL simulation using the loosely-coupled scheme. This simulation involves  $I_2$ -He injection into a primary stream of excited singlet oxygen. The problem was run with Roe flux differencing, third-order accuracy and viscous effects including molecular diffusion. Mach number and small signal gain contours for this case are shown in Fig. 8.

## 3.7 Conclusions

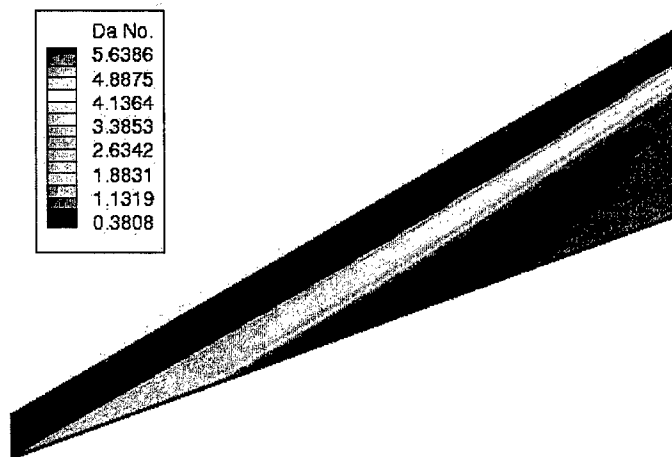
We have examined an number of steady-state flows and compared results with loosely-coupled/operator splitting methods to fully-coupled results. The result compare well. The primary potential of this approach is in the area of inexpensive explicit schemes. With the source-term stiffness removed, the memory and extra computational expense of fully-coupled implicit schemes can be avoided. We



(a) Temperature.

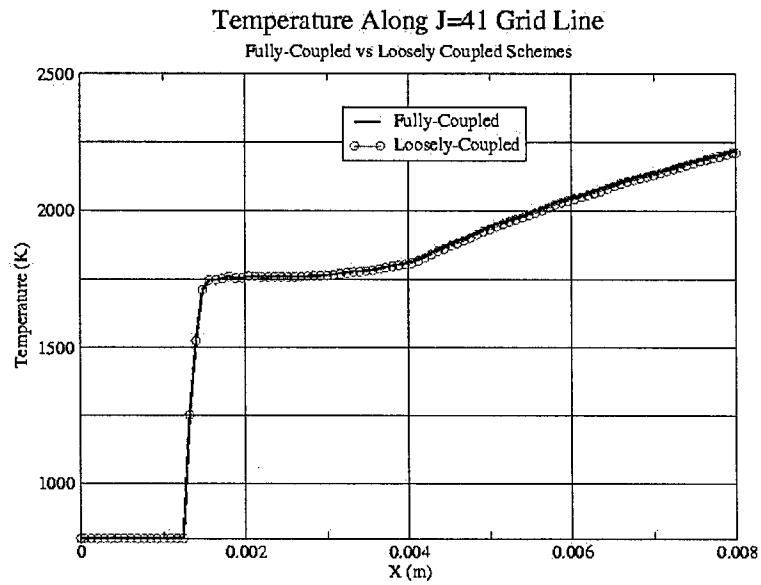


(b)  $H_2O$  Mass fraction.

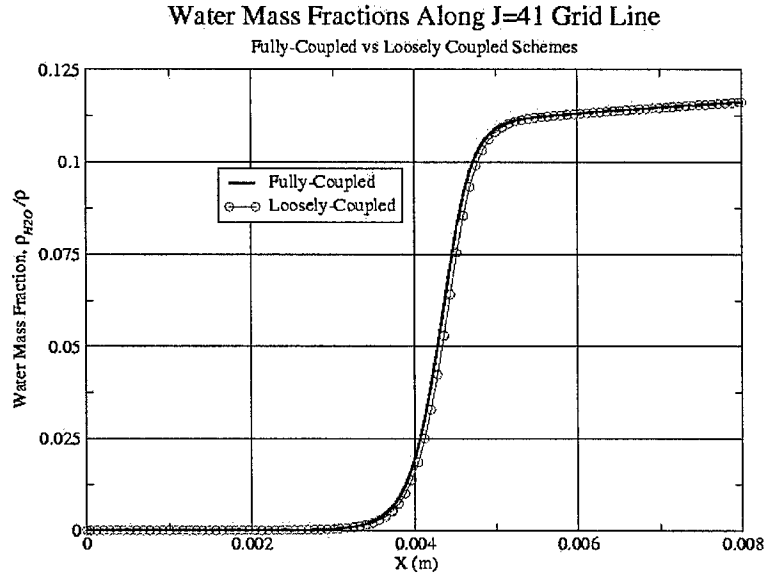


(c) Damkohler number.

Figure 5: Contours of temperature,  $H_2O$  mass fractions, and  $Da$  number for the hydrogen-air wedge flow.



(a) Temperature.



(b)  $H_2O$  Mass fraction.

Figure 6: Line plots of temperature and  $H_2O$  mass fractions for hydrogen-air wedge flow.

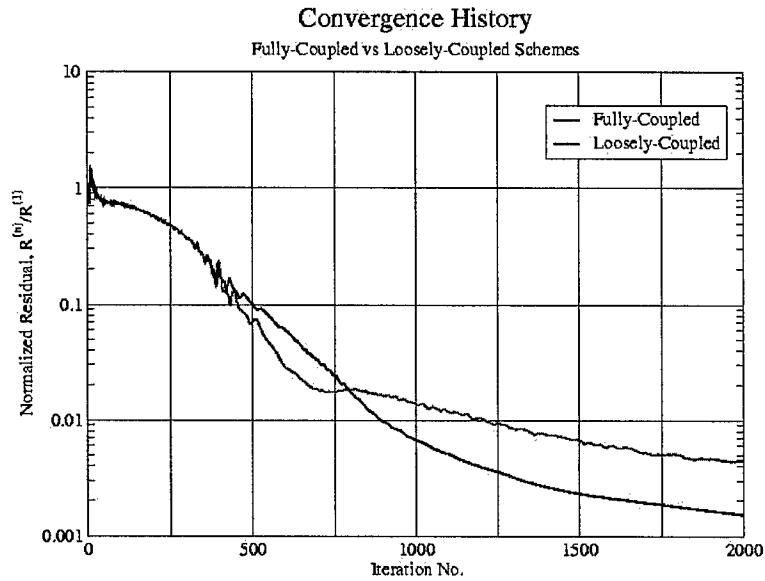
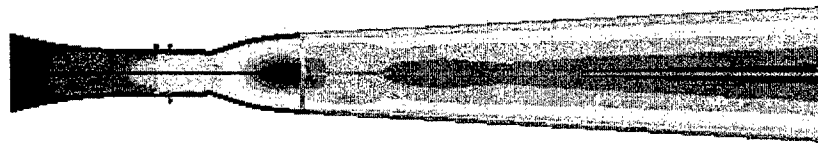
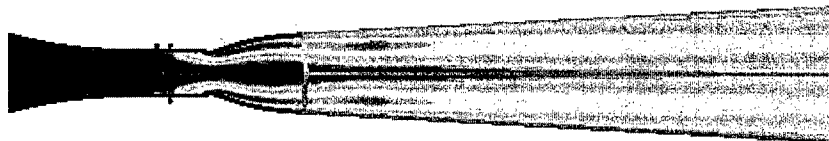


Figure 7: Convergence history for fully and loosely-coupled schemes for the hydrogen-air wedge flow.



(a) Mach number.



(b) Small signal gain.

Figure 8: Contour plots of temperature and small signal gain for 2-D COIL simulation.

have been able to obtain solutions with finite-rate chemistry using explicit methods for the chemical system. While these solutions require more iterations than implicit calculations, they become much more efficient as the number of species increases. Although this work is focused at reducing the computational resources for chemical laser calculations, these methods are also applicable to hydrocarbon fuels which can involve 50 or more chemical species. Detailed chemical mechanisms for hydrocarbon fuels are continually progressing in their accuracy, however, their direct use in calculations is prohibitive, and reduced models must be used.

## 4 Personnel Supported

Dr. William M. Eppard at AeroSoft, Inc.

## 5 Publications

Damkohler Limiting of Chemical Time Scales - Paper Number : AIAA-2005-1400

## 6 Interactions/Transitions

Dr. Eppard attended the AFOSR Review meeting in August, 2005. The improved capabilities in GASP v4 will provide an immediate impact on laser analysis efforts at AFRL/DE and are also being used at Northrup Grumman.

## 7 New Discoveries, Inventions, or Patent Disclosures

None.

## 8 Honors/Awards

None.

## References

- [1] R. A. Baurle, T. Mathur, M. R. Gruber, and K. R. Jackson. "A Numerical and Experimental Investigation of a Scramjet Combustor for Hypersonic Missile Applications". AIAA Paper 98-3121, 34<sup>th</sup> AIAA/ASME/ASE/ASEE Joint Propulsion Conference and Exhibit, July 13-15 1998.
- [2] J. P. Drummond, R. C. Rogers, and M. Y. Hussaini. "A Detailed Numerical Model of a Supersonic Reacting Mixing Layer". AIAA Paper 86-1427, AIAA/ASME/SAE/ASEE 22<sup>nd</sup> Joint Propulsion Conference, June 16-18, 1986.
- [3] S. R. Turns. **An Introduction to Combustion**. McGraw-Hill, 2000.